Electronic Supplementary Information for

In-Situ Reconstruction Enhanced Dual-Site Catalysis towards Nitrate Electroreduction to Ammonia

Jiahao Cai,[†a] Shuaibo Qin,[†b] Muhammad Awais Akram, [†a] Xiangdie Hou,[c] Peng Jin,[b] Feng Wang,[a] Botao Zhu,[a] Xiaohong Li,*[c] Lai Feng*[a]*

[a]College of Energy, Soochow Institute for Energy and Materials InnovationS, Soochow University, Suzhou 215006, China. E-mail: fenglai@ suda.edu.cn

[b]School of Materials Science and Engineering, Hebei University of Technology, Tianjin 300130, China. E-mail: china.peng.jin@gmail.com

[c]College of Chemistry, Chemical Engineering and Materials Science, the Key Lab of Health Chemistry and Molecular Diagnosis of Suzhou, Soochow University, Suzhou 215006, China. E-mail: lxh83@suda.edu.cn

[†]These authors contribute equally to this work.

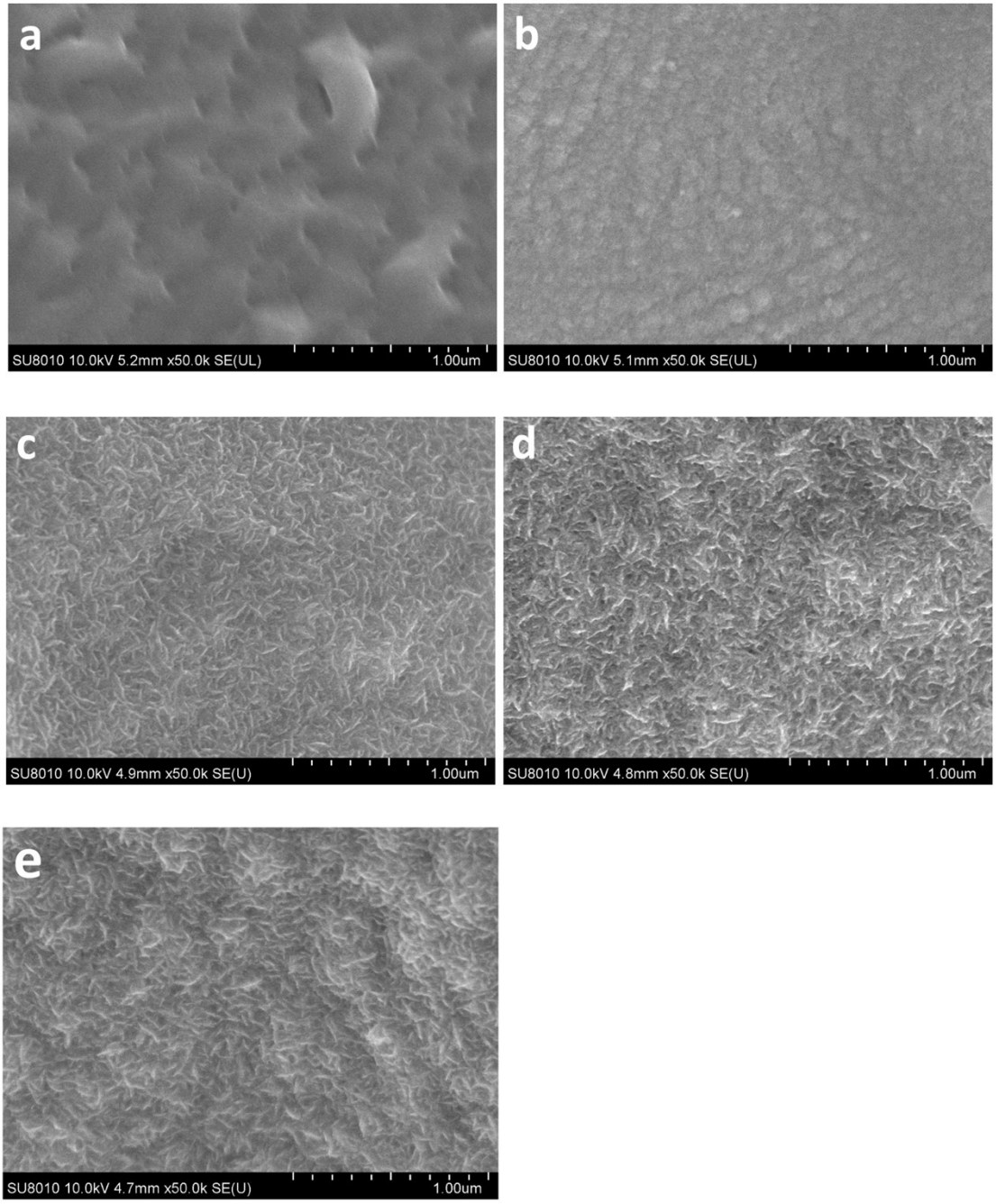

Figure S1. SEM images of (a) CuO_x (b) RuO_x, (c) $Cu_1Ru_1O_x$, (d) $Cu_3Ru_1O_x$ and (e) $Cu_5Ru_1O_x$ grown on nickel foam (NF).

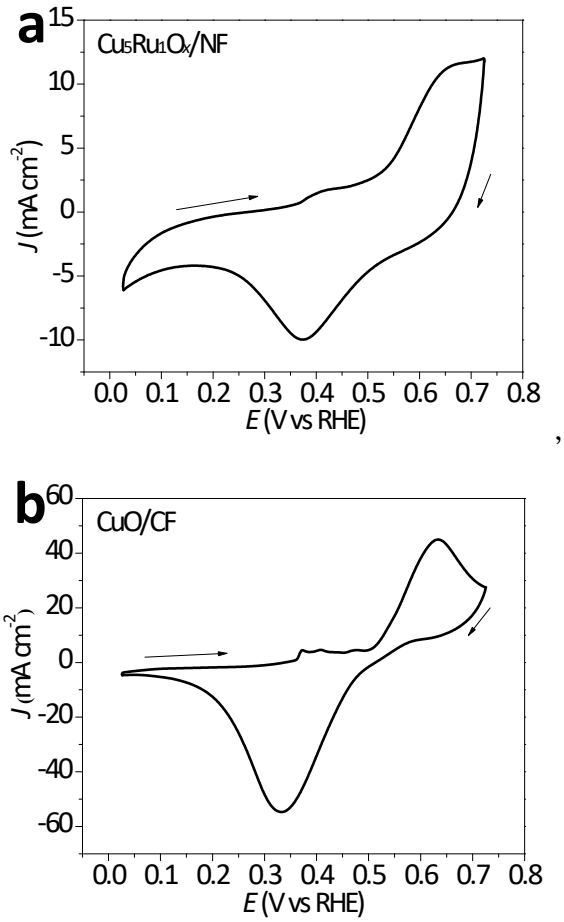

Figure S2. CV profiles recorded in 1 M KOH: (a) the as-synthesized $Cu_5Ru_1O_x$ and (b) the CuO grown on copper foam (CF) as reference. Note: Both CV profiles reveal a reduction process in the range of 0.25 ~ 0.45 V (*vs* RHE), which could be attributed to the reduction of Cu^{2+} to Cu^{+} according to the literature report (*J. Phys. Chem. B* **1999,** *103,* 357-365). The reference sample CuO/CF was prepared according to the literature (*Electrochimica Acta,* 2016, **210**, 639–645).

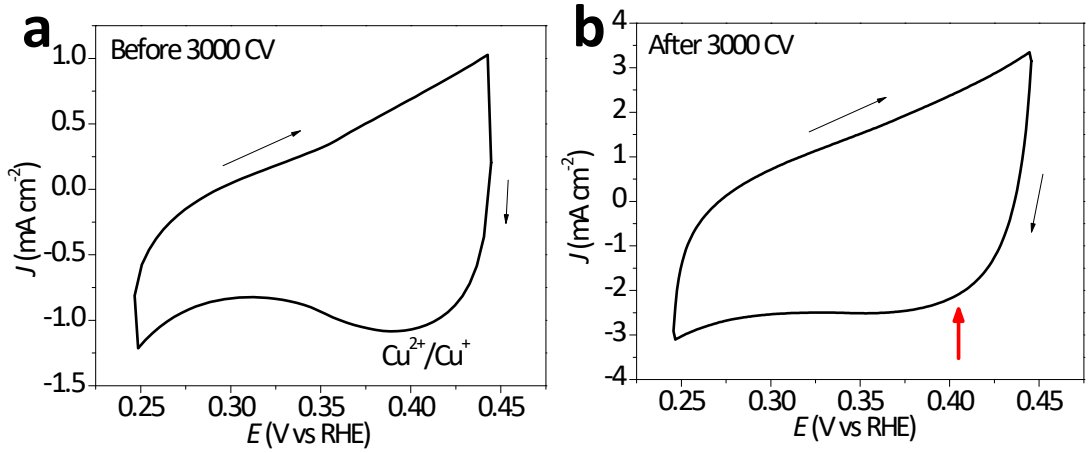

Figure S3. CV profiles for Cu_5RuO_x (a) before and (b) after 3000 CV potential sweeps in 1 M KOH (scan rate: 100 mV s^{-1}). Note: After 3000 CV potential sweeps, the current density remarkably increases, indicative of enhanced double-layer

capacitance (C_{dl}) and in line with the following measurements (see Figure S11). Meanwhile, after 3000 CV potential sweeps, the reduction peak at around 0.4 V *vs* RHE becomes almost negligible, indicative of the suppressed content of Cu^{2+}.

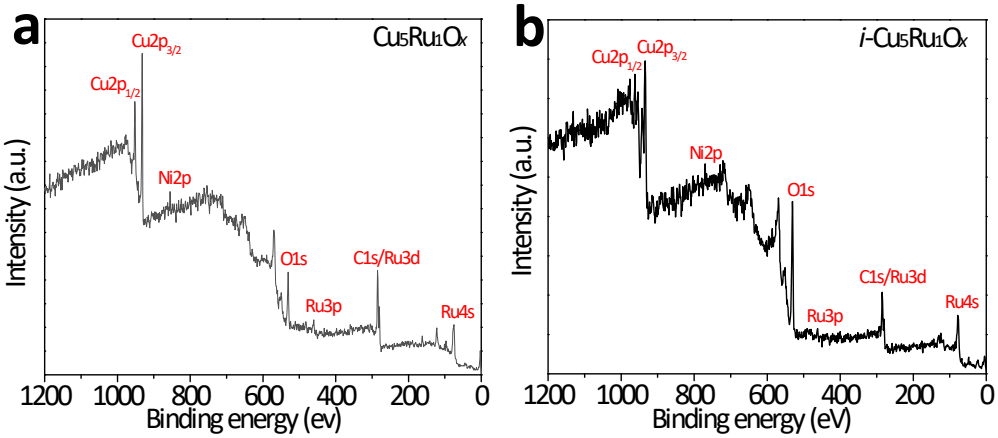

Figure S4. XPS survey of (a) $Cu_5Ru_1O_x$ and (b) *i*-Cu_5RuO_x.

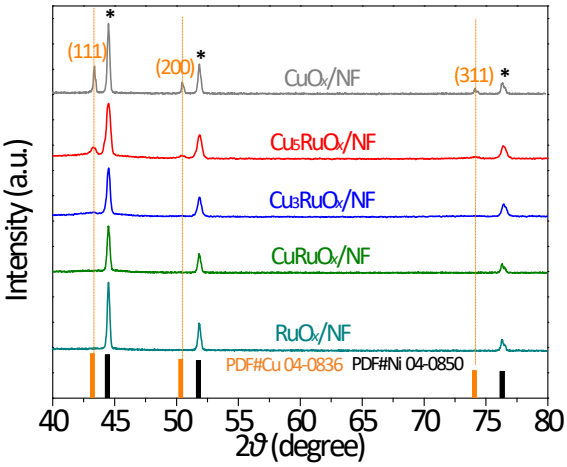

Figure S5. XRD spectra of CuO_x, RuO_x and $CuRuO_x$ series.

The reference CuO_x displays remarkable diffraction peaks at 2θ = 43.4°, 50.5° and 74.1°, corresponding to the Cu (111), (200) and (311) planes, respectively. With the increase of Ru content, these diffraction peaks become weaken for Cu_5RuO_x and almost negligible for Cu_3RuO_x and $CuRuO_x$, indicating that the crystallinity is decreasing upon the introduction of Ru species. Note that Ru^0 has an atom radius similar to that of Cu^0 (1.32 versus 1.28 Å), so the 2θ values of the diffraction peaks of Cu remain almost constant upon the Ru introduction.

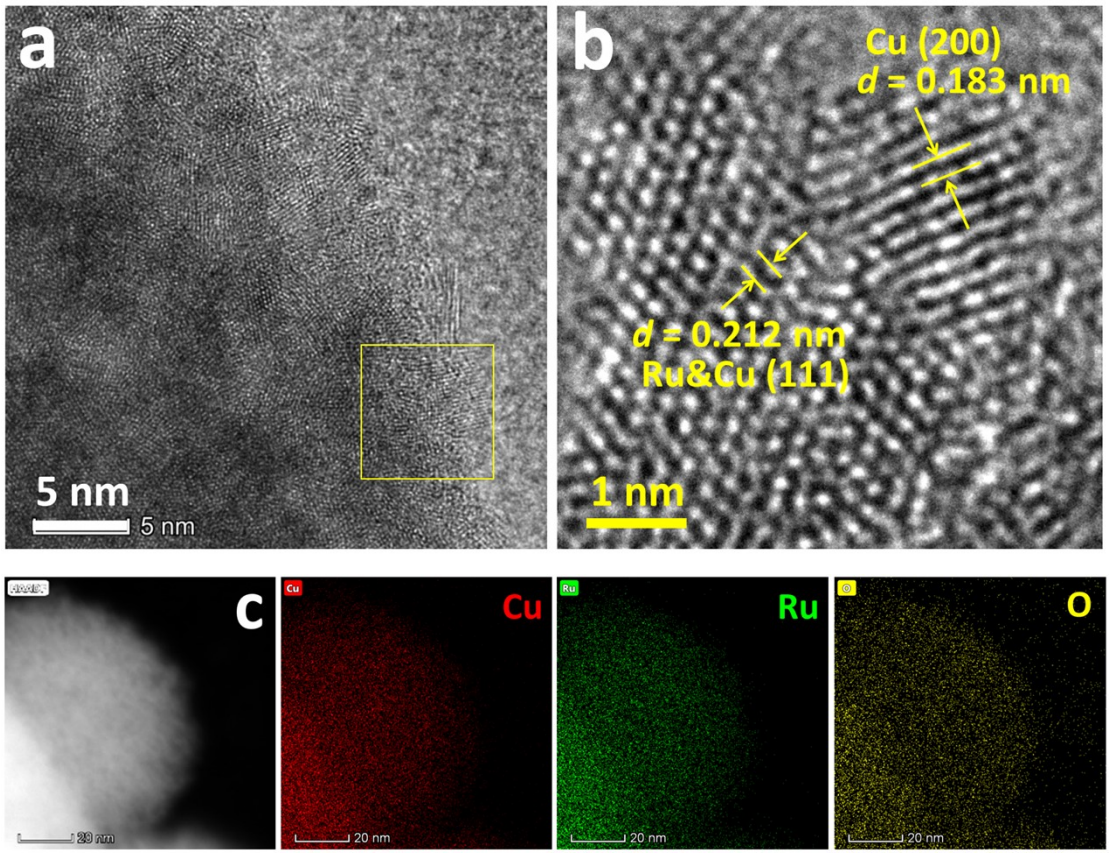

Figure S6. (a,b) HR-TEM, (c) HAADF and element mapping images of $Cu_5Ru_1O_x$. Scale bars in HAADF and element mapping image indicate 20 nm.

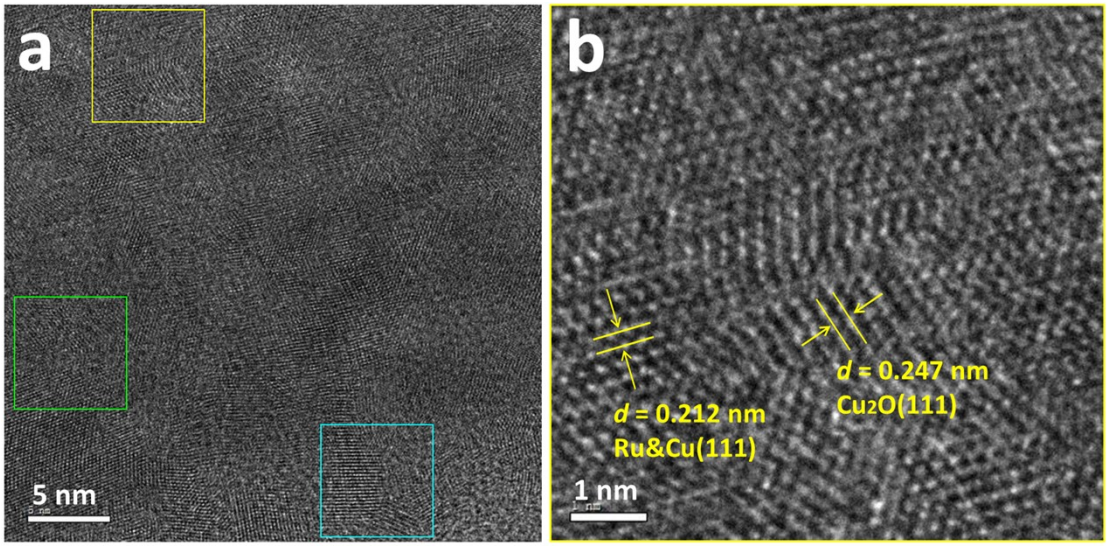

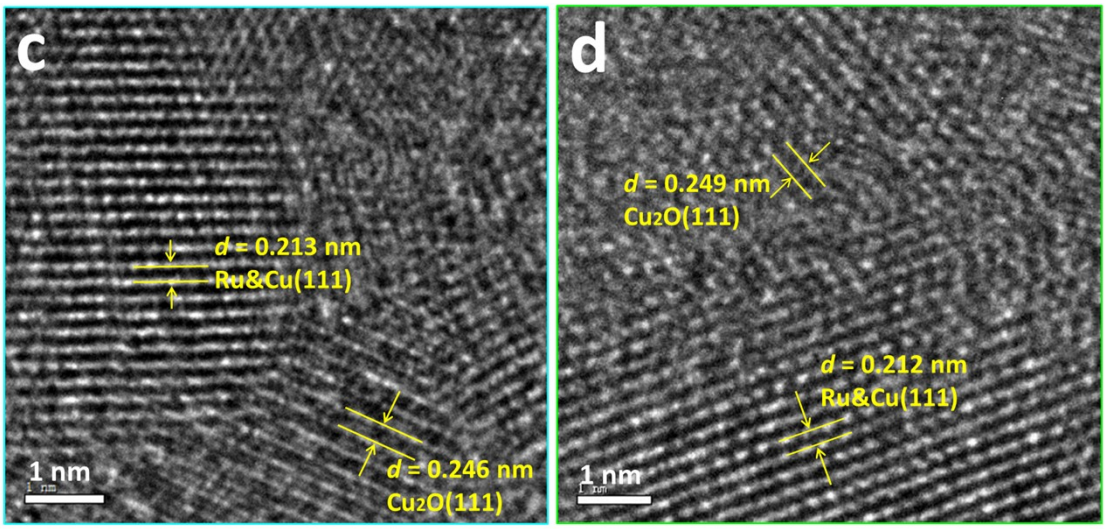

Figure S7. (a-d) HR-TEM images of *i*-$Cu_5Ru_1O_x$, showing the presence of multiple Ru&Cu/Cu_2O heterojunctions over a random domain.

Figure S8. Photo of the PTFE made H-cell for HER and *e*-NRA measurements.

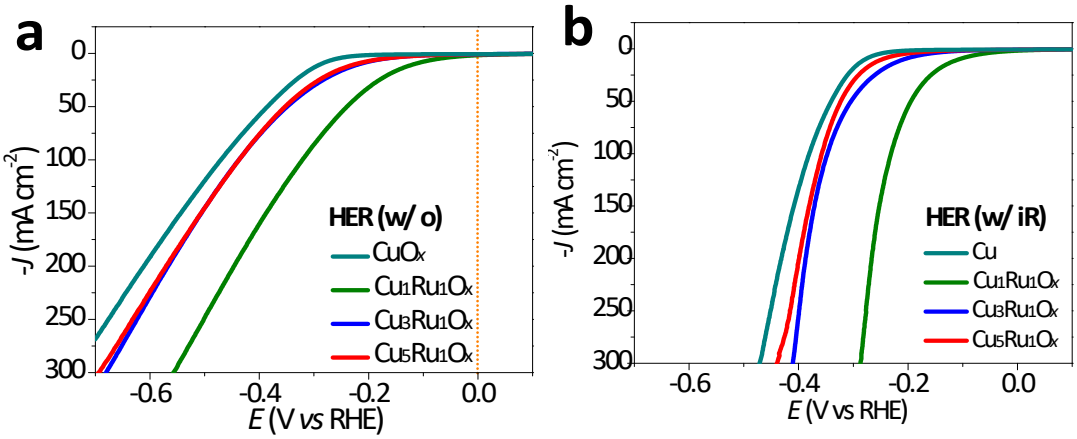

Figure S9. Polarization curves of CuO_x and $CuRuO_x$ series towards HER (1 M KOH) (a) without and (b) with iR compensation.

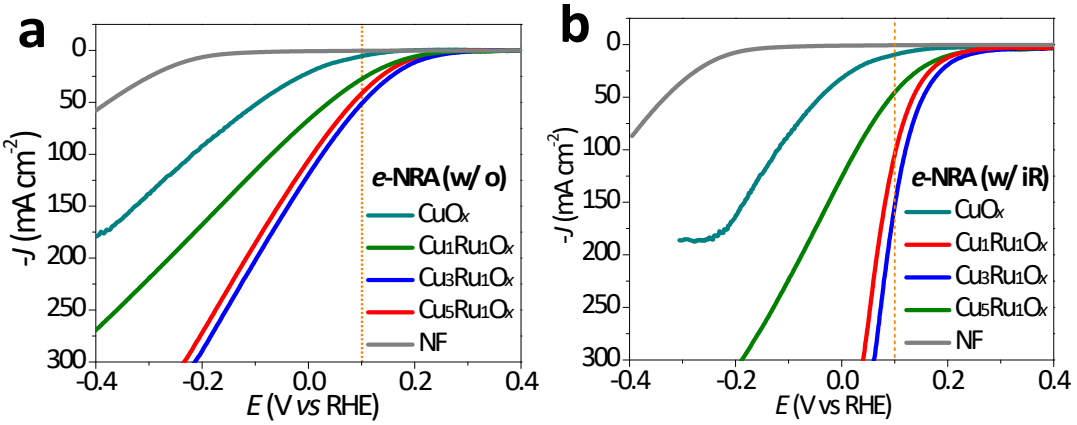

Figure S10. Polarization curves of CuO_x and $CuRuO_x$ series towards *e*-NRA (1 M KOH with 0.1 M KNO_3) (a) without and (b) with iR compensation.

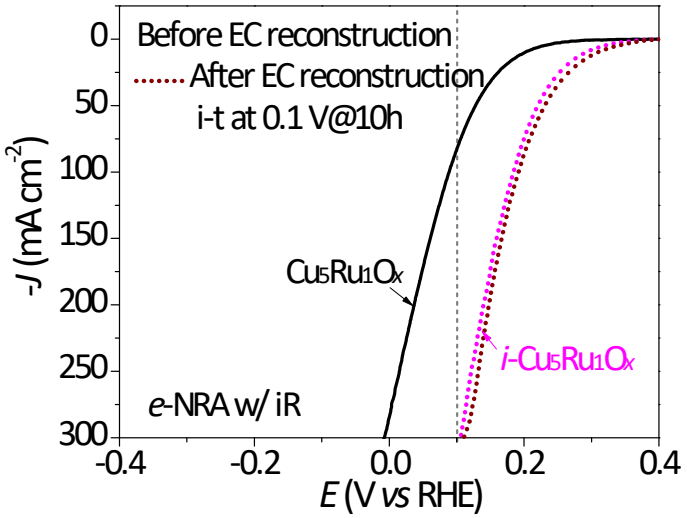

Figure S11. Polarization curves of $Cu_5Ru_1O_x$ and *i*-$Cu_5Ru_1O_x$ towards *e*-NRA (1 M KOH with 0.1 M KNO_3) with iR compensation.

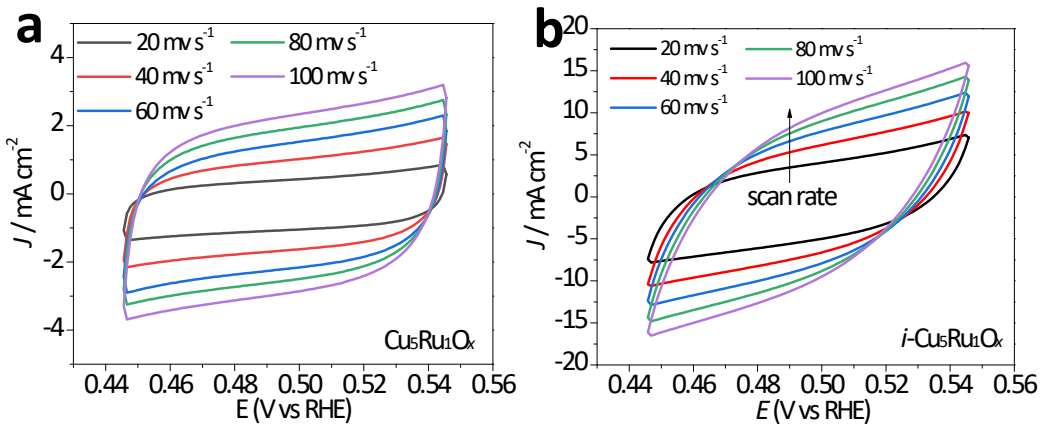

Figure S12. ECSA measurements of the catalysts. (a,b) The cyclic voltammetry profiles obtained for $Cu_5Ru_1O_x$ and *i*-$Cu_5Ru_1O_x$ at the sweep rates of 20, 40, 60, 80 and 100 mV s^{-1}, respectively. See Figure 4c for the determination of double layer capacitance (C_{dl}) for each catalyst.

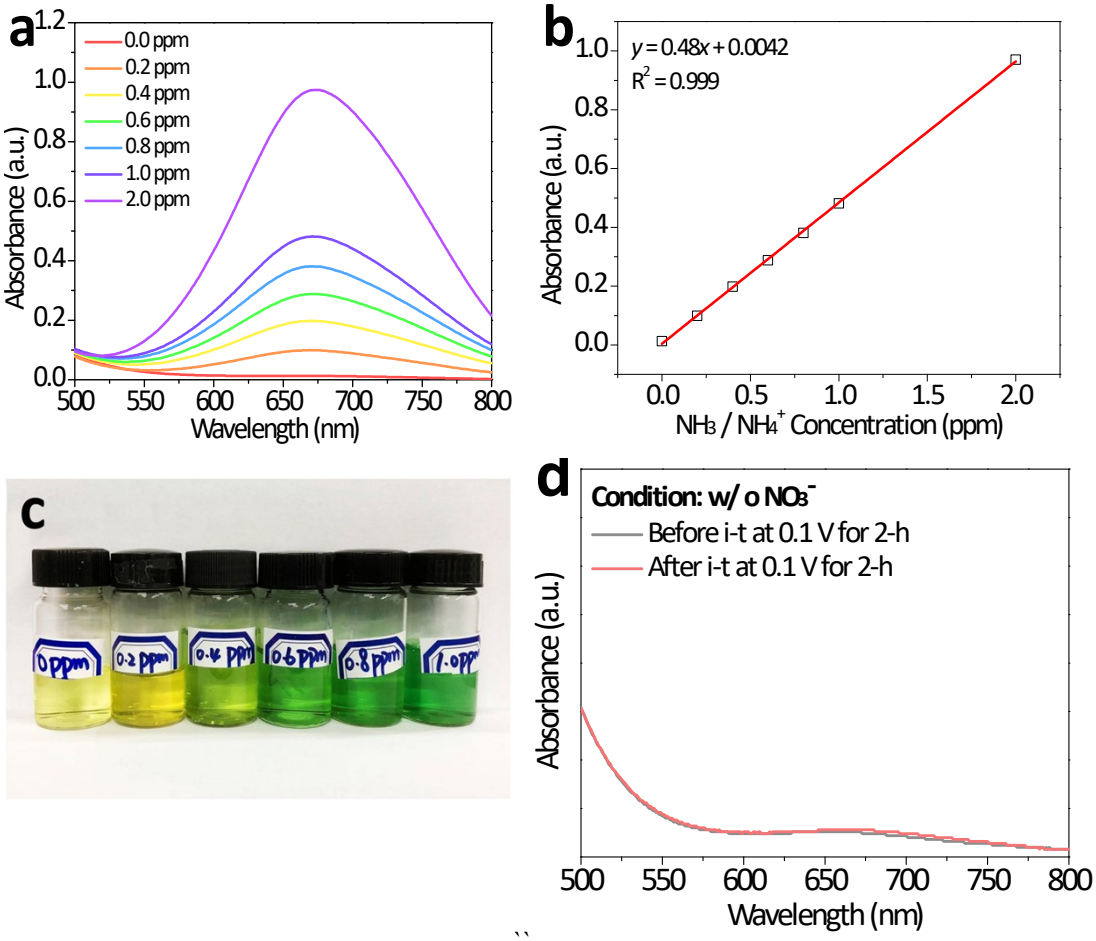

Figure S13. Standard calibration of ammonia concentration against absorbance for indophenol blue method. (a) Visible adsorption spectra of standard solutions with different ammonia concentrations. (b) The linear standard curve for the calculation of ammonia production. (c) Photo of standard solutions with different ammonia concentrations. (d) Visible adsorption spectra of the electrolytes obtained before and

after the *i-t* process at 0.1 V (vs RHE) with 1 M KOH-only (without KNO_3). Note: no feature absorbance at around 680 nm indicates no production of NH_3.

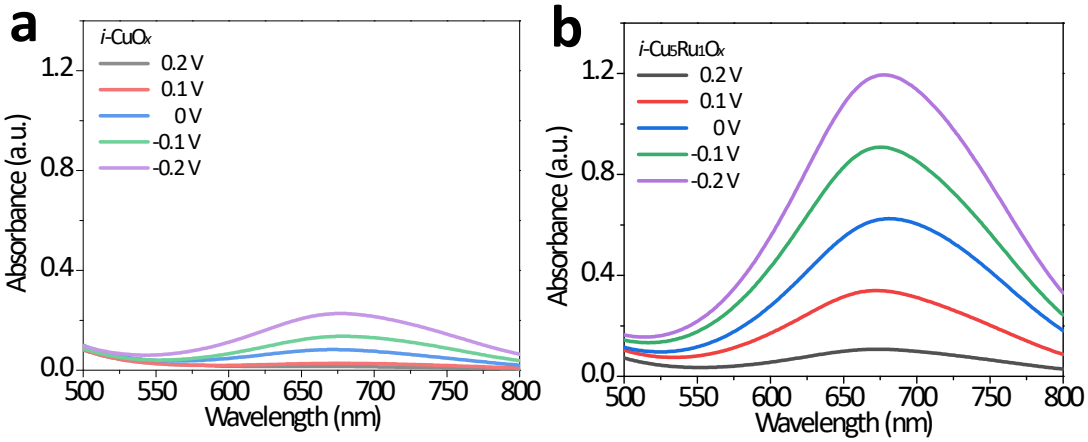

Figure S14. Absorption spectra of the electrolyte (diluted by 2-fold) after *e*-NRA at different potentials on the catalysts of (a) *i*-CuO_x and (b) *i*-$Cu_5Ru_1O_x$ for 1-h using the methodology of indophenol.

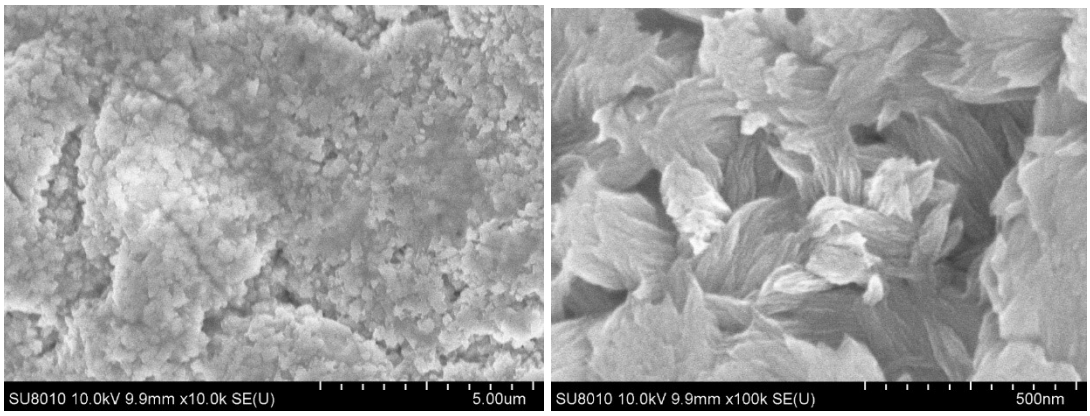

Figure S15. SEM images of *i*-CuO_x, which was derived from CuO_x via the similar *in-situ* electro-reduction.

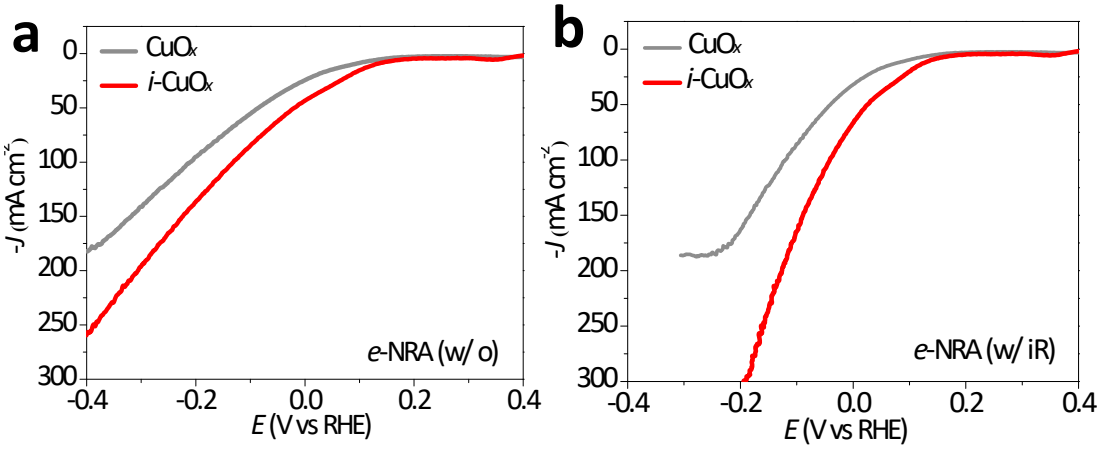

Figure S16. Polarization curves of CuO_x and *i*-CuO_x series towards *e*-NRA (1 M KOH with 0.1 M KNO_3) (a) without and (b) with iR compensation.
Note: The improved *e*-NRA activity of *i*-CuO_x could be attributed to the transformation of CuO species to Cu_2O during the electrochemical reconstruction.

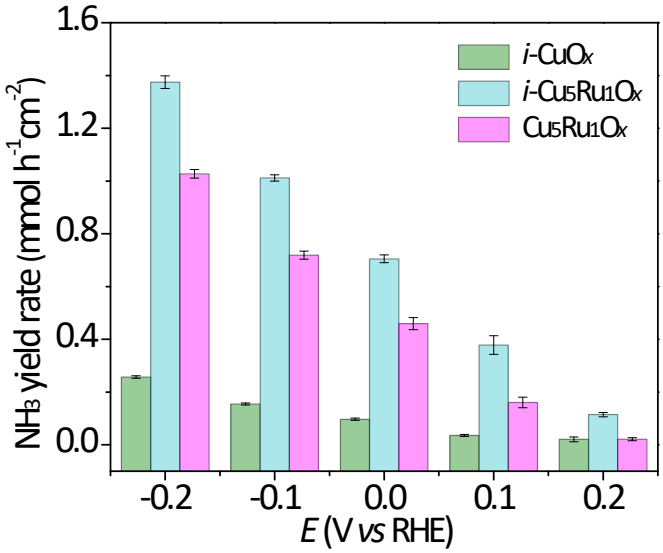

Figure S17. NH_3 yield rate of the *e*-NRA at different working potentials on the catalysts of *i*-CuO_x, *i*-$Cu_5Ru_1O_x$ and $Cu_5Ru_1O_x$ for 1-h.

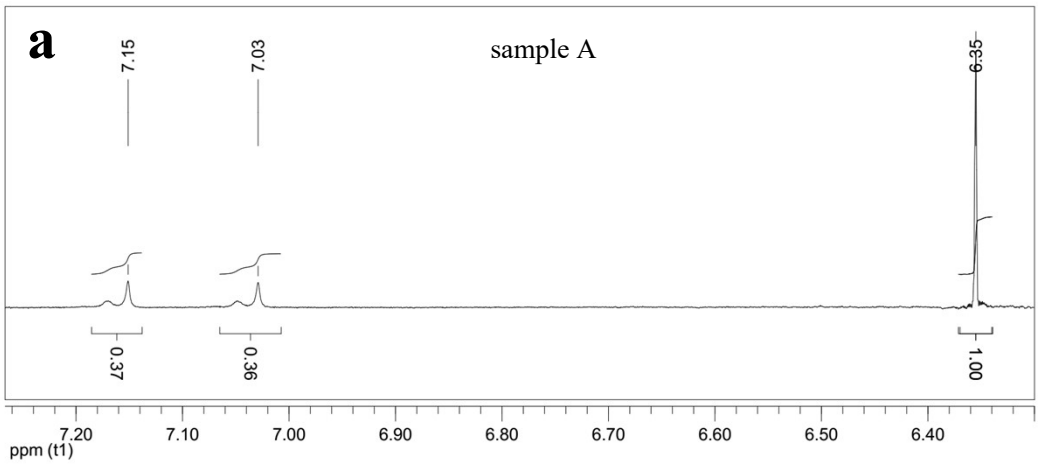

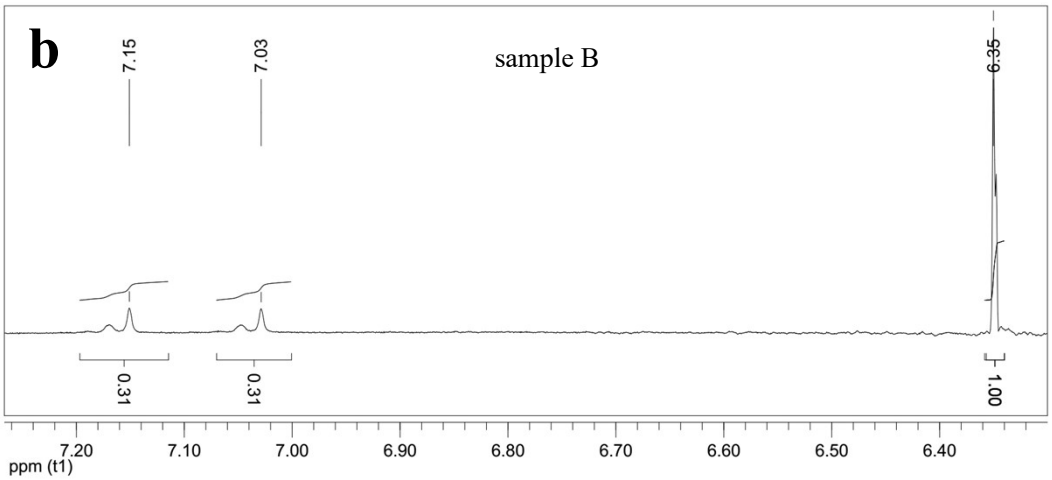

Figure S18. ^{1}H NMR spectra of the electrolyte obtained from the continuous *e*-NRA at 0.1 V (vs RHE) using $^{15}NO_3^-$ as nitrate. (a) To prepare sample A, *e*-NRA proceeded at 0.1 V for 1-h and the electrolyte was diluted for 3.9-fold; (b) To prepare sample B, *e*-NRA proceeded at 0.1 V for 1.5-h and the electrolyte was diluted for 6.5-fold.
Note: To prepare sample A, 300 µL electrolyte was combined with 600 µL DI water, 50 µL H_2SO_4 (1 M), 100 µL maleic acid (500 ppm) and 120 µL D_2O. So, total volume is 1170 µL and the electrolyte was diluted by 3.9 fold.
To prepare sample B, 180 µL electrolyte was combined with 720 µL DI water, 50 µL H_2SO_4 (1 M), 100 µL maleic acid (500 ppm) and 120 µL D_2O. So, total volume is 1170 µL and the electrolyte was diluted by 6.5 fold.

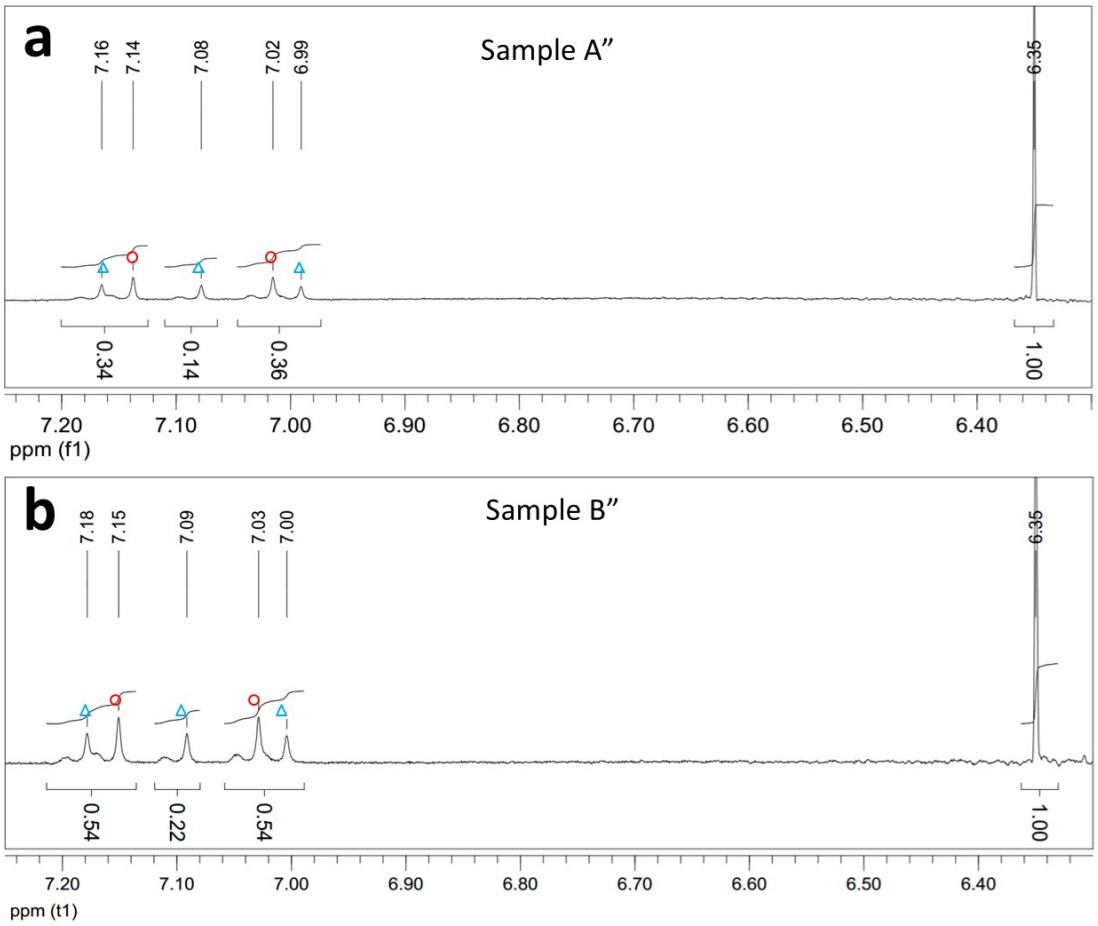

Figure S19. ^{1}H NMR spectra of the electrolyte obtained from the continuous *e*-NRA at 0.1 V (vs RHE) using $^{15}NO_3^-/^{14}NO_3^-$ (1/1) as nitrate. (a) To prepare sample A", *e*-NRA proceeded at 0.1 V for 1-h and the electrolyte was diluted for 4.5-fold; (b) To prepare sample B", *e*-NRA proceeded at 0.1 V for 1.5-h and the electrolyte was diluted for 4.5-fold. The NH_3 FE was calculated to be 90.1% and 90.0%, respectively. The red circles represent ^{1}H doublet of $^{15}NH_4^+$, while the blue triangles represent ^{1}H triplet of $^{14}NH_4^+$.

Note: To prepare sample A", 1 mL electrolyte was combined with 500 µL H_2SO_4 (1 M), then 300 µL neutralized electrolyte was combined with 600 µL DI water, 100 µL maleic acid (500 ppm) and 120 µL D_2O. So, total volume is 1150 µL and the electrolyte was diluted by 4.5 fold.
Sample B" was prepared following the same procedure.

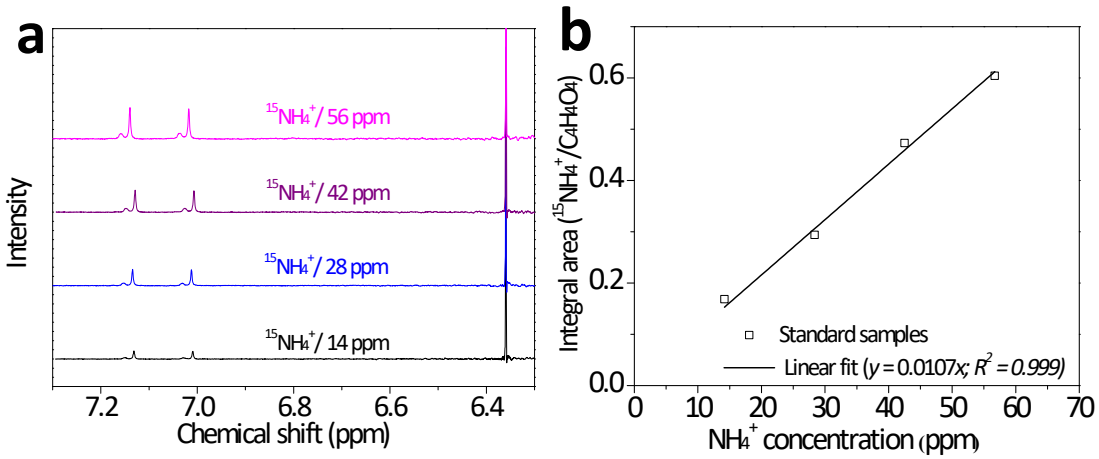

Figure S20. (a) ^{1}H NMR spectra of $^{15}NH_4^+$ ($(^{15}NH_4)_2SO_4$ in a mixed solution of H_2O/D_2O with *v/v* of 1.05/0.12) with different concentrations; (b) Standard plot of integral area ($^{15}NH_4^+/C_4H_4O_4$) against $^{15}NH_4^+$ concentration.

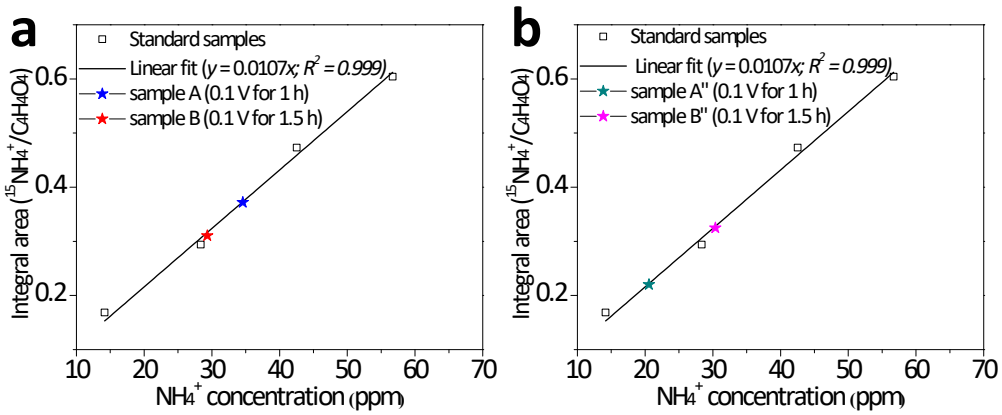

Figure S21. (a) Determination of NH_3 concentration of sample A or B based on the standard plot; (b) Determination of NH_3 concentration of sample A'' or B'' based on the standard plot.

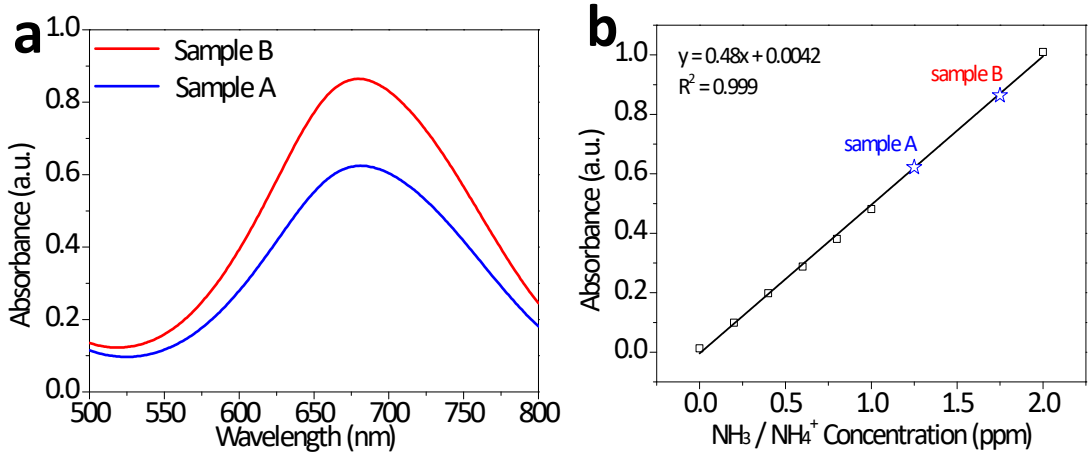

Figure S22. The determination of NH_3 FE by using indophenol blue method: (a) visible absorption spectra of samples A and B; (b) Standard plot of NH_3 concentrations against their absorbance, in which the concentrations of samples A and B were determined accordingly.

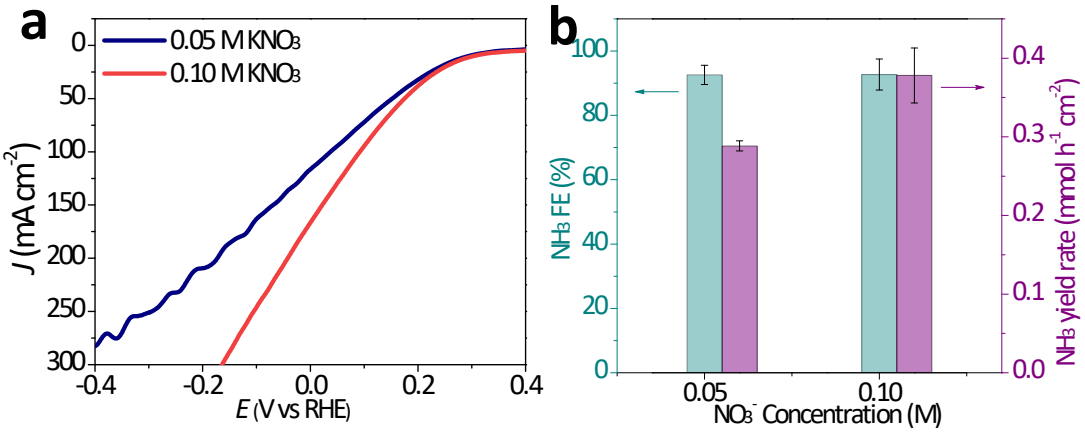

Figure S23. (a) Polarization curves of e-NRA with different KNO_3 concentrations (0.05 and 0.10 M) on the catalysts of *i*-$Cu_5Ru_1O_x$, and (b) corresponding NH_3 yield rates and NH_3 FE.

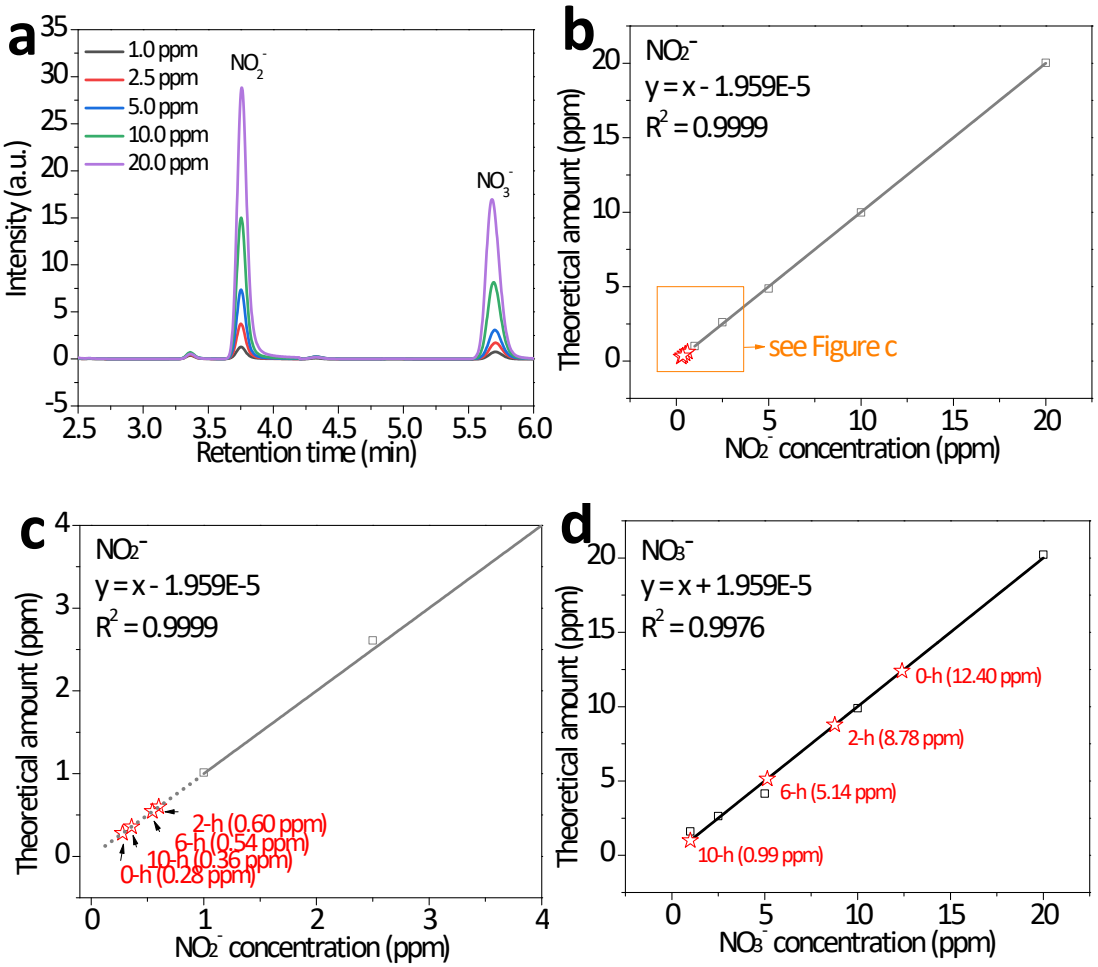

Figure S24. Ion chromatography (IC) profiles of (a) standard solutions containing different concentrations of NO_3^- and NO_2^-; (b,c,d) Standard plots of NO_2^- and NO_3^- concentrations against their integrated area in IC profile, in which the concentrations of samples were determined accordingly. Note: In b-d, the theoretical amount refers to the data given by IC linear analysis.

Note: To prepare samples for IC test, the electrolytes (20 μL) before and after *e*-NRA (at 0.1 V *vs* RHE for 2, 6, 10-h) were diluted by 500 times. The concentrations of NO_3^- and NO_2^- (ppm) in the diluted samples were determined based on the standard calibration plots based on IC analysis. Accordingly, the concentrations of NO_3^- and NO_2^- (ppm) in the electrolytes could be calculated.

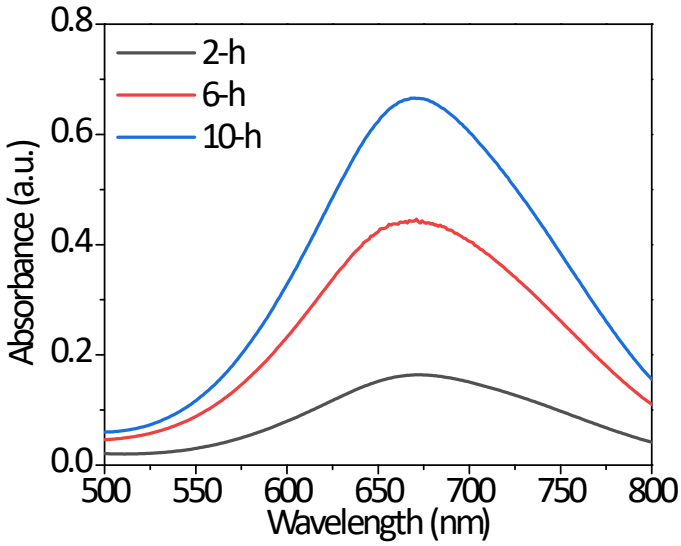

Figure S25. Visible absorption spectra of the electrolytes (diluted by 10-fold) obtained at 2, 6, 10-h during a continuous *e*-NRA at 0.1 V (*vs* RHE).

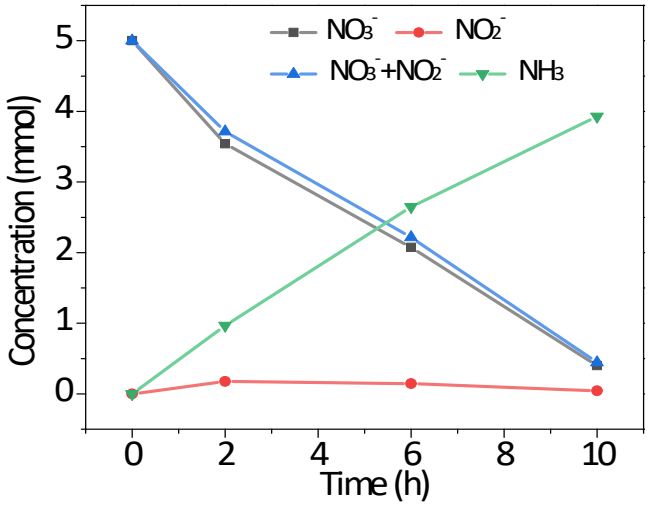

Figure S26. Time-dependent concentration change of NH_3, NO_3^-, NO_2^- and their combination during *e*-NRA at 0.1 V (*vs* RHE).

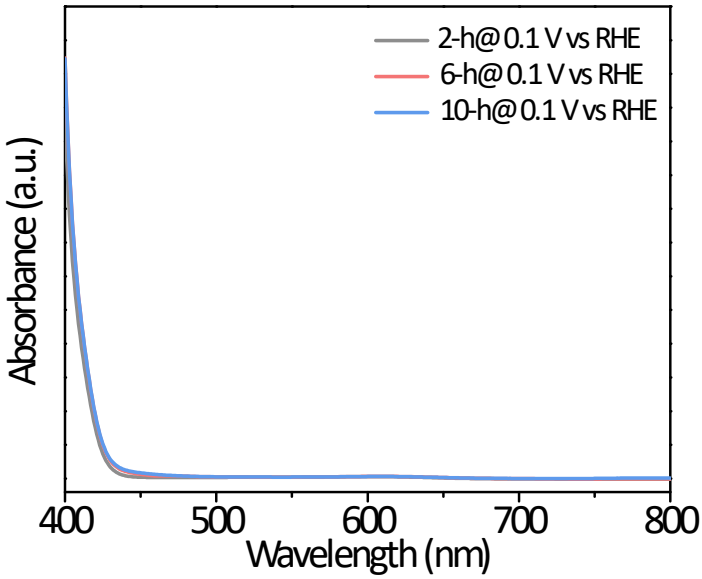

Figure S27. Visible absorption spectra of the electrolytes stained with Watt and Chrisp test reagents after *e*-NRA at 0.1 V (*vs* RHE) for 2, 6, 10 -h on *i*-$Cu_5Ru_1O_x$.

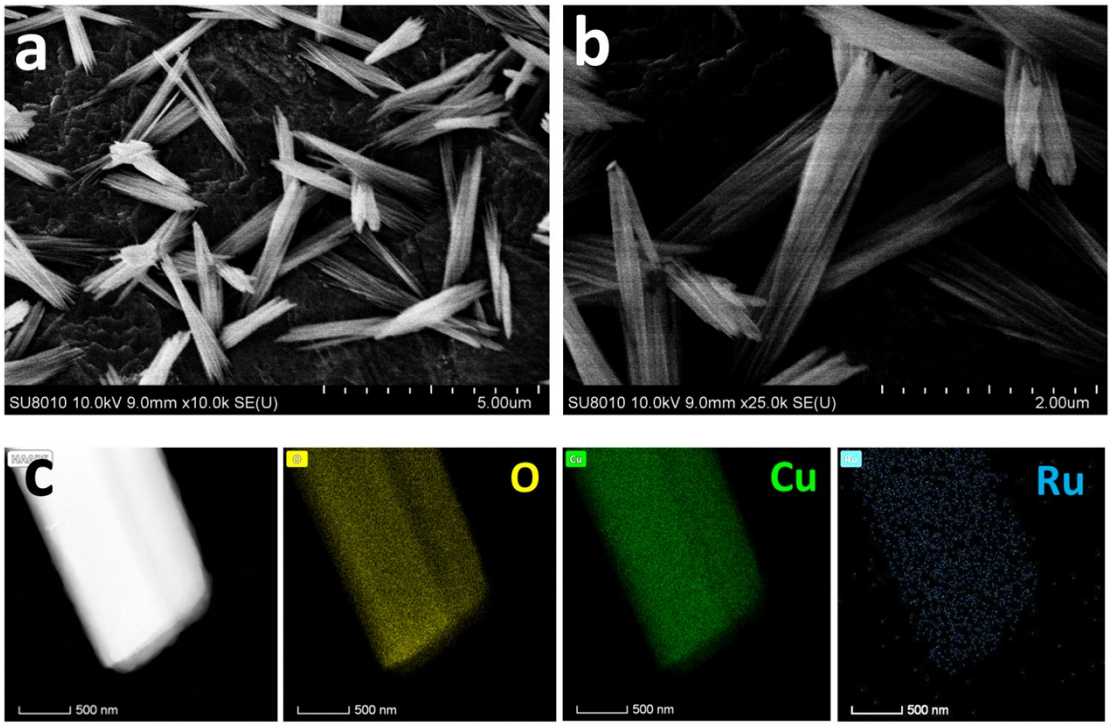

Figure S28. (a,b) SEM image and (c) HAADF-STEM and EDX mapping of *i*-$Cu_5Ru_1O_x$ after the consecutive *e*-NRA at 0.1 V (*vs* RHE) for 10-h.

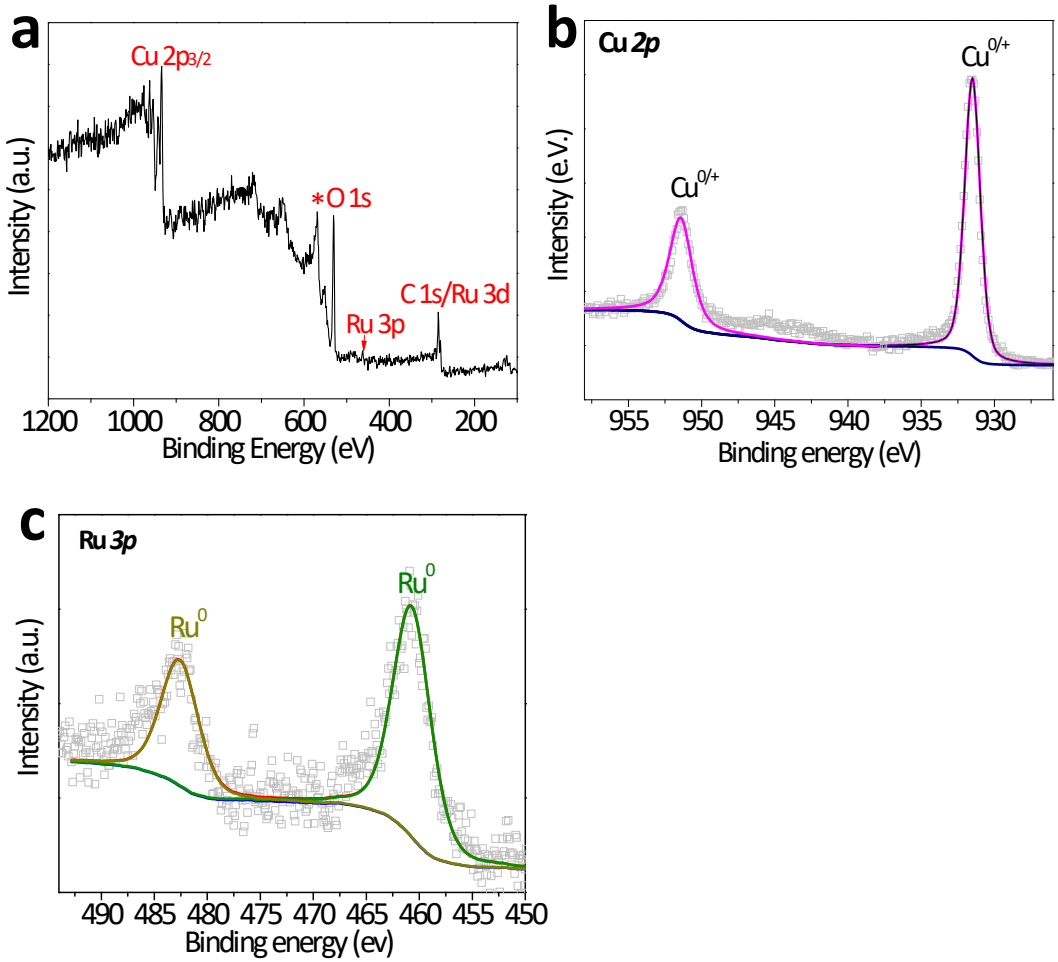

Figure S29. XPS spectra of *i*-$Cu_5Ru_1O_x$ after the consecutive *e*-NRA at 0.1 V (*vs* RHE) for 10-h.

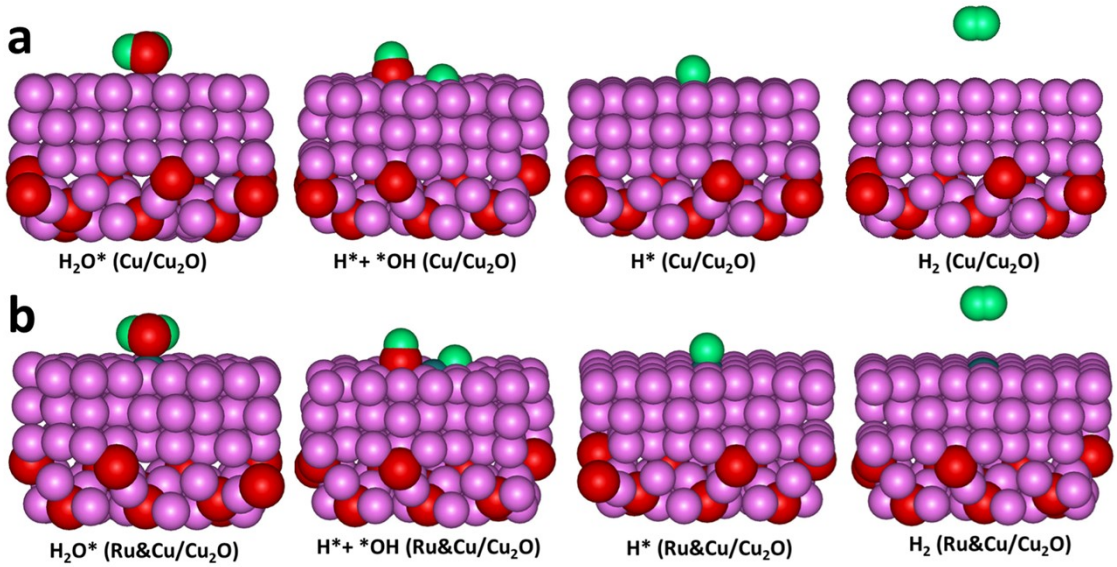

Figure S30. DFT-optimized intermediates for HER over different catalyst models: (a) Cu/Cu_2O and (b) $Ru\&Cu/Cu_2O$.

Computational details:

According to the literatures,[1-3] the NO_3^- reduction reaction on the catalyst surface was simulated by considering the following elementary steps (* indicates active site):

$$* + NO_3^- + 6H_2O + 8e^- \rightarrow *NO_3 + 6H_2O + 9e^- \quad (1)$$

$$*NO_3 + 6H_2O + 9e^- \rightarrow *NO_2 + 5H_2O + 2OH^- + 7e^- \quad (2)$$

$$*NO_2 + 5H_2O + 2OH^- + 7e^- \rightarrow *NO + 4H_2O + 4OH^- + 5e^- \quad (3)$$

$$*NO + 4H_2O + 4OH^- + 5e^- \rightarrow *N + 3H_2O + 6OH^- + 3e^- \quad (4)$$

$$*N + 3H_2O + 6OH^- + 3e^- \rightarrow *NH + 2H_2O + 7OH^- + 2e^- \quad (5)$$

$$*NH + 2H_2O + 7OH^- + 2e^- \rightarrow *NH_2 + H_2O + 8OH^- + e^- \quad (6)$$

$$*NH_2 + H_2O + 8OH^- + e^- \rightarrow *NH_3 + 9OH^- \quad (7)$$

$$*NH_3 + 9OH^- \rightarrow * + NH_3(g) + 9OH^- \quad (8)$$

$$\text{Total reaction: } * + NO_3^- + 6H_2O + 8e^- \rightarrow * + NH_3(g) + 9OH^- \quad (9)$$

The following Gibbs free energies were then defined:

$$G_1 = G(*) + G(NO_3^-) + 6G(H_2O) \quad (10)$$

$$G_2 = G(*NO_3) + 6G(H_2O) \quad (11)$$

$$G_3 = G(*NO_2) + 5G(H_2O) + 2G(OH^-) \quad (12)$$

$$G_4 = G(*NO) + 4G(H_2O) + 4G(OH^-) \quad (13)$$

$$G_5 = G(*N) + 3G(H_2O) + 6G(OH^-) \quad (14)$$

$$G_6 = G(*NH) + 2G(H_2O) + 7G(OH^-) \quad (15)$$

$$G_7 = G(*NH_2) + G(H_2O) + 8G(OH^-) \quad (16)$$

$$G_8 = G(*NH_3) + 9G(OH^-) \quad (17)$$

$$G_9 = G(*) + G(NH_3) + 9G(OH^-) \quad (18)$$

The free energy change for each step along the reaction path was thus calculated by:

$$\Delta G = G_n - G_{n-1} = \Delta E + \Delta ZPE - T\Delta S \quad (19)$$

where n=1-9 corresponds to the above G_1-G_9, ΔZPE and ΔS are the changes in zero-point energy and entropy, respectively, after the intermediate adsorption and can be obtained from the vibrational frequency calculations (with adsorbates relaxed and substrates fixed) and standard thermodynamic data. T is the temperature (298.15 K).

To avoid the calculation of charged NO_3^-, the HNO_3 (g) was chosen as reference. The adsorption free energy of NO_3^- (ΔG_{*NO3}) was calculated following the literatures:[4-6]

$$\Delta G_{*NO3} = G_{*NO3} - G_* - G_{HNO3(g)} + 1/2G_{H2(g)} + \Delta G_{correct} \quad (20)$$

where G_{*NO3}, G_*, $G_{HNO3(g)}$ and $G_{H2(g)}$ are the free energies of NO_3 adsorbed on the catalyst surface, the pristine catalyst, HNO_3 in gas state, H_2 in gas state, respectively. $\Delta G_{correct}$ is the correction to the free energy and is 0.392 eV (0.075 + 0.317 = 0.392), in which 0.075 eV is the free energy change for $HNO_3(g) \rightarrow HNO_3(l)$, and 0.317 eV is the free energy change for $HNO_3(l) \rightarrow H^+ + NO_3^-$ according to the CRC Handbook of Chemistry and Physics.[7]

On the other hand, to obtain the free energy diagram for HER over different catalyst models in Fig. 6e, the free energy change was calculated by using the computational hydrogen electrode (CHE) model, which defines that the free energy of a proton-electron pair is equal to half of the free energy of a H_2 molecule.

Note: As shown in Figure 6a, the final desorption of NH_3 is more endothermic on the

Ru&Cu/Cu_2O than Cu/Cu_2O. This result indicates that the desorption of NH_3 on Ru&Cu/Cu_2O is slower than that on Cu/Cu_2O, which may result in lower surface concentration (θ) of unoccupied active sites and hence slow down the reaction rate. However, it has been revealed that overall rate (r) expression may be relatively complex. A simple heterogeneous catalytic reaction below is taken as a typical example.

A + * = *A(ads) (1)

*A(ads) = *B(ads) (2)

*B(ads) = B + * (3)

Here, * denotes the active site, *A(ads) the adsorbed reactant, *B(ads) the adsorbed product.

The reaction rate expression even for this simple mechanism, using the law of mass action and the simplification that reactions (1) and (3) are close to steady state, is relatively complicated (as shown by G. F. Froment, K. B. Bischoff, and J. De Wilde in *Chemical Reactor Analysis and Design*):[8]

$$\gamma = \frac{\theta(c_A - \frac{c_B}{k})}{(k_1 + k_2 c_A + k_3 c_B)}$$

In this equation, besides above mentioned θ and r, c_A, c_B are the concentrations of reagent A and product B, respectively. K, k_1, k_2 and k_3 are constant.

So, the concentrations of reagent and product are also key factors in determining the overall reaction rate. In our case, if the NO_3^- and NH_3 concentrations are sufficiently low, the effect of low k_3 may be negligible. This issue remains to be explored in the further work.

References in **Computational details:**

1. Y. Wang, A. Xu, Z. Wang, et al. Enhanced nitrate-to-ammonia activity on copper–nickel alloys via tuning of intermediate adsorption. *J. Am. Chem. Soc.,* 2020, **142**, 5702-5708.
2. Y. Wang, X. Qin, M. Shao, First-principles mechanistic study on nitrate reduction

reactions on copper surfaces: Effects of crystal facets and pH. *J. Catal.,* 2021, **400**, 62-70.

3. H. Yin, Z. Chen, S. Xiong, et al. Alloying effect-induced electron polarization drives nitrate electroreduction to ammonia. *Chem Catal*., 2021, **1**, 1088-1103.
4. F. Calle-Vallejo, M. Huang, J. B. Henry, et al. Theoretical design and experimental implementation of Ag/Au electrodes for the electrochemical reduction of nitrate. *Phys. Chem. Chem. Phys.*, 2013, **15**, 3196-3202.
5. Niu H., Zhang Z., Wang X., et al. Theoretical Insights into the Mechanism of Selective Nitrate-to-Ammonia Electroreduction on Single-Atom Catalysts. *Adv. Funct. Mater.*, 2021, **31**, 2008533.
6. J. X. Liu, D. Richards, N. Singh, et al. Activity and selectivity trends in electrocatalytic nitrate reduction on transition metals. *ACS Catal*., 2019, **9**. 7052-7064.
7. D. R. Lide, CRC *Handbook of Chemistry and Physics* (90th Ed.), 2010.
8. G. F. Froment, K. B. Bischoff, and J. De Wilde in *Chemical Reactor Analysis and Design.* (3rd Ed.), 2011.

Table S1. The highest FE_{NH_3} *and* corresponding working potentials reported in the literature**.**

Catalyst	***Highest*** FE_{NH_3}	***Potential*** [a]	***Electrolyte***	***Ref.***
Cu/Cu_2O NWAs	95.8%	-0.85 (V vs RHE)	0.5 M Na_2SO_4 + 200 ppm NO_3^-- N	1
$PdCu/Cu_2O$ hybrid	94.32%	-0.80 (V vs RHE)	0.5 M Na_2SO_4 + 100 ppm NO_3^-- N	2
$Cu_{50}Ni_{50}$/PTFE	99±1%	-0.15 (V vs RHE)	1 M KOH + 0.1 M KNO_3	3
Ru-ST-12	96%	-0.2 (V vs RHE)	1 M KOH + 1 M KNO_3	4
O-Cu–PTCDA	85.9%	-0.4 (V vs RHE)	500 ppm KNO_3 + 0.1 M PBS	5
Co-NAs	≥ 97 %	0.06 ~ -0.24 (V vs. RHE)	1 M KOH + 0.1 M KNO_3	6
	≥ 96 %	-0.3 ~ -0.6 (V vs. RHE)	0.5 M Na_2SO_4 + 0.1 M NO_3^-- N	
TiO_{2-x}	85%	-1.6 (V vs. SCE)	0.5 M Na_2SO_4 + 50 ppm NO_3^-- N	7
Fe SAC	74.9%	-0.85 (V vs RHE)	0.1 M Na_2SO_4 +	8

			0.5 M KNO_3	
	86%	-0.21 (V vs RHE, 2h)	1 M KOH + 0.1 M KNO_3	
Ru&Cu/Cu_2O	> 95%	0.1 (V vs RHE)	1 M KOH + 0.1 M KNO_3	This work

[a] The working potential for *e*-NRA, where the highest FE_{NH_3} was achieved.

References in Table S1.

1. Y. Wang, W. Zhou, R. Jia, Y. Yu and B. Zhang, *Angew Chem. Int. Ed.*, 2020, **59**, 5350-5354.
2. H. Yin, Z. Chen, S. Xiong, J. Chen, C. Wang, R. Wang, Y. Kuwahara, J. Luo, H. Yamashita, Y. Peng and J. Li, *Chem. Catal.*, 2021, **1**, 1088-1103.
3. Y. Wang, A. Xu, Z. Wang, L. Huang, J. Li, F. Li, J. Wicks, M. Luo, D. H. Nam, C. S. Tan, Y. Ding, J. Wu, Y. Lum, C. T. Dinh, D. Sinton, G. Zheng and E. H. Sargent, *J. Am. Chem. Soc.*, 2020, **142**, 5702-5708.
4. J. Li, G. Zhan, J. Yang, F. Quan, C. Mao, Y. Liu, B. Wang, F. Lei, L. Li, A. W. M. Chan, L. Xu, Y. Shi, Y. Du, W. Hao, P. K. Wong, J. Wang, S. X. Dou, L. Zhang and J. C. Yu, *J. Am. Chem. Soc.*, 2020, **142**, 7036-7046.
5. G.-F. Chen, Y. Yuan, H. Jiang, S.-Y. Ren, L.-X. Ding, L. Ma, T. Wu, J. Lu and H. Wang, *Nat. Energy*, 2020, **5**, 605-613.
6. X. Deng, Y. Yang, L. Wang, X. Z. Fu and J. L. Luo, *Adv. Sci.,* 2021, **8**, 2004523.
7. R. Jia, Y. Wang, C. Wang, Y. Ling, Y. Yu and B. Zhang, *ACS Catal.*, 2020, **10**, 3533-3540.
8. Z. Y. Wu, M. Karamad, X. Yong, Q. Huang, D. A. Cullen, P. Zhu, C. Xia, Q. Xiao, M. Shakouri, F. Y. Chen, J. Y. T. Kim, Y. Xia, K. Heck, Y. Hu, M. S. Wong, Q. Li, I. Gates, S. Siahrostami and H. Wang, *Nat. Commun.*, 2021, **12**, 2870.

Table S2. ICP-AES analysis results of $CuRuO_x$ series**.**

Catalyst	Cu (wt%)	Ru (wt%)	Cu/Ru molar ratio
$Cu_1Ru_1O_x$	18.17	14.15	2.03
$Cu_3Ru_1O_x$	27.28	7.01	6.15
$Cu_5Ru_1O_x$	31.54	4.91	10.15
i-$Cu_5Ru_1O_x$	25.44	4.89	8.21

Table S3. HER performance of $CuRuO_x$ series and CuO_x.

HER	CuO_x	$Cu_1Ru_1O_x$	$Cu_3Ru_1O_x$	$Cu_5Ru_1O_x$
E (J = 2 mA.cm^{-2}) (mV *vs* RHE) Without IR compensation	-215.4	-10.4	-108.4	-100.4
E (J = 2 mA.cm^{-2}) (mV *vs* RHE) With IR compensation	-213.6	-86	-107	-98.6
E (J = 100 mA.cm^{-2}) (mV *vs* RHE) Without IR compensation	-470.4	-321.4	-437.4	-43.74
E (J = 100 mA.cm^{-2}) (mV *vs* RHE) With IR compensation	-380.4	-231.2	-347.3	-347.2

Table S4. Impedance spectra fitting results for the alkaline *e*-NRA of $Cu_5Ru_1O_x$ and *i*-$Cu_5Ru_1O_x$.

catalyst	R_S (Ω cm^2)	Yo (Ω^{-1} cm^{-2} sn)	n	R_{CT} (Ω cm^2)
$Cu_5Ru_1O_x$	0.90	0.0042	0.86	11.59
i- $Cu_5Ru_1O_x$	0.80	0.042	0.72	3.56

Table S5. Time-dependent amounts of NO_3^-, NO_2^- and their combination during continuous *e*-NRA on *i*-$Cu_5Ru_1O_x$ at 0.1 V (*vs* RHE) under single-pass condition, calculated based on IC data. NO_3^- conversion and NO_2^- selectivity are calculated accordingly.[a]

Time (h)	Residual $n(NO_3^-)$ (mmol)	Generated $n(NO_2^-)$ (mmol)	Total anion (mmol)	NO_3^- conversion (%)	NO_2^- selectivity (%)	$FE_{NO_2^-}$ (%)
0	5.000	/	5.000	/	/	/
2	3.539	0.1743	3.866	29.22	11.93	4.28
6	2.074	0.1441	2.370	58.52	4.92	1.28
10	0.3996	0.04310	0.5949	92.01	0.94	0.25

[a]NO_3^- conversion and NO_2^- selectivity were calculated using the following equations.

$$Conversion = \frac{\Delta C_{NO_3^-}}{C_0} = \frac{n_{total}(NO_3^-) - n(NO_3^-)_{residual}}{n(NO_3^-)_{total}} \times 100\%$$

$$Selectivity = \frac{C}{\Delta C_{NO_3^-}} = \frac{n(NO_2^- \text{ or } NH_4^+)_{residual}}{n(NO_3^-)_{total} - n(NO_3^-)_{residual}} \times 100\%$$

$$FE_{NO_2^-} = \left(2 \times F \times n_{NO_2^-}\right) / \left(M_{NO_2^-} \times Q\right) \times 100\%$$

Table S6. Time-dependent amounts of NH_3 during continuous *e*-NRA on *i*-$Cu_5Ru_1O_x$ at 0.1 V (*vs* RHE) under single-pass condition, calculated based on absorption data. NH_3 yield rate, selectivity and FE are calculated accordingly.

Time (h)	Produced $n(NH_3)$ (mmol)	NH_3 yield rate (mmol h^{-1} cm^{-2})	NH_3 Selectivity (%)	FE_{NH_3} (%)
2	0.9679	0.4840	66.26	94.96
6	2.646	0.4410	90.44	93.96
10	3.930	0.3929	85.42	91.20